Reverse-chiral response of two $\mathcal{T}$-symmetric optical systems hosting conjugate exceptional points

Arnab Laha, Sibnath Dey, and Somnath Ghosh*

Unconventional Photonics Laboratory, Department of Physics, Indian Institute of Technology Jodhpur, Rajasthan-342037, India

(Received 11 August 2021; accepted 12 January 2022; published 3 February 2022)

Exceptional points (EPs) are a special kind of singularity that appear as topological defects in parameter-dependent open systems. Here we propose the concept of conjugate EPs, where a level-repulsion phenomenon between two coupled complex states can occur in the vicinity of a square-root branch point, which is analytically associated with the presence of two complex conjugate EPs. Depending on the iteration parameter, two corresponding levels are analytically connected via one of two conjugate EPs. Here, we report the hosting of two conjugate EPs in two complementary equivalent systems connected with time-reversal ($\mathcal{T}$) symmetry by using the framework of a gain-loss assisted dual-mode planar optical waveguide. We establish that if the complex potential of any system hosts an EP, then the $\mathcal{T}$-symmetric potential of the same system can host the associated conjugate EP. Owing to the EP-aided nonadiabatic population transfer based on device chirality, the reverse-chiral responses of two $\mathcal{T}$-symmetric devices have been explored in the context of an asymmetric-mode-conversion process. The proposed scheme has the potential to open up a credible platform to study the physics of EPs in $\mathcal{T}$-symmetric systems.

DOI: 10.1103/PhysRevA.105.022203

I. INTRODUCTION

The presence of exceptional points (EPs) is one of the distinct non-Hermitian features of nonconservative systems [1]. EPs are the branch-point singularities appearing in the system's parameter space, for which at least two coupled eigenvalues and the corresponding eigenvectors coalesce simultaneously, and hence the Hamiltonian of the underlying systems becomes defective, referring to the EP as a topological defect [2,3]. Over the last two decades, the optics and photonics domains have been presenting EPs as an intrinsic tool for manipulating the light-matter interactions [4,5] towards a wide range of astonishing applications, such as ultrasensitive optical sensing [6,7], topological energy transfer [8], state flipping [9–11], lasing and coherent perfect absorption [12,13], parametric instability [14], and so on. The dynamical parametric variation around an EP enables nonadiabatic (time-asymmetric) light dynamics enriched with an asymmetric-mode-conversion mechanism in any length-dependent guided-wave optical geometry [15–17], where nonreciprocal light transmission with enhanced isolation ratio can also be achieved in the presence of nonlinearity [18,19]. Such nontrivial light guidance is essentially governed by the chirality of the associated EP [20–22].

The presence of an EP is inextricably associated with the avoided resonance crossing (ARC) phenomenon among the complex states with crossing and anticrossing of their frequencies and widths (essentially, the real and imaginary parts, respectively) [20,23]. At the elementary level, without any loss of generality for higher (or infinite)-dimensional problems, a level repulsion phenomenon can elementarily be explained by considering a two-level Hamiltonian $\mathcal{H}(\lambda)$, having the form $H_0 + \lambda H_p$ as

$$\mathcal{H}(\lambda) = \begin{bmatrix} \varepsilon_1 & 0 \\ 0 & \varepsilon_2 \end{bmatrix} + \lambda \begin{bmatrix} \omega_1 & \kappa_1 \\ \kappa_2 & \omega_2 \end{bmatrix}. \tag{1}$$

Here, the passive system H_0, consisting of two distinct levels ε_j ($j = 1$ and 2), is subjected to a parameter-dependent perturbation H_p, where ω_j and κ_j ($j = 1$ and 2) are the perturbation parameters. λ is a complex iteration parameter that signifies the perturbation strength. Now, the eigenvalues of $\mathcal{H}(\lambda)$ can be written as

$$E_{1,2}(\lambda) = \frac{(\varepsilon_1 + \varepsilon_2) + \lambda(\omega_1 + \omega_2)}{2} \pm C; \tag{2a}$$

$$C = \left[\left(\frac{\varepsilon_1 - \varepsilon_2}{2} \right)^2 + \lambda^2 \left\{ \left(\frac{\omega_1 - \omega_2}{2} \right)^2 + \kappa_1 \kappa_2 \right\} + \frac{\lambda}{2} (\varepsilon_1 - \varepsilon_2)(\omega_1 - \omega_2) \right]^{1/2}. \tag{2b}$$

Now, if we consider all real parameters in both H_0 and H_p, then the overall $\mathcal{H}(\lambda)$ defines a Hermitian system for a real λ. For a trivial consideration of $\kappa_{1,2} = 0$, the spectrum of such a system can be written by two lines, $E_j(\lambda) = \varepsilon_j + \lambda \omega_j$ ($j = 1$ and 2), which intersect at a degeneracy point and exhibit a conventional singularity (say, a diabolic point) at $\lambda_c = -(\varepsilon_1 - \varepsilon_2)/(\omega_1 - \omega_2)$. However, λ_c disappears upon the consideration of $\kappa_{1,2} \neq 0$, where one can observe the non-Hermitian coupling between two levels, $E_{1,2}(\lambda)$, via ARC-type interactions for a complex λ ($= \lambda_R + i\lambda_I$). Such an ARC can be associated with the locating of a branch point singularity, i.e., an EP. For a chosen variation of λ_R, different kind of special ARCs with crossing and anticrossing of real and imaginary parts (or vice versa) of E_1 and E_2 can be

*somiit@rediffmail.com

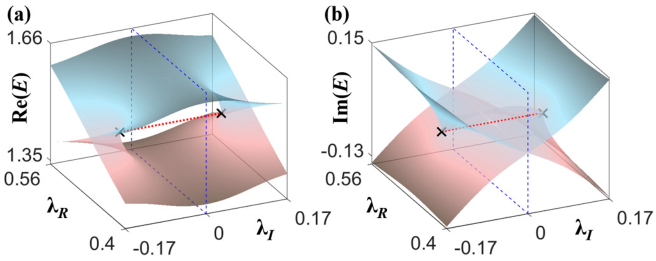

FIG. 1. Distribution of Riemann surfaces associated with (a) Re(E) and (b) Im(E) concerning the simultaneous variations of λ_R and λ_I (in the vicinity of the interaction regime) for a specifically chosen set of parameters in $\mathcal{H}(\lambda)$, where two black crosses represent the formation of two conjugate EPs. The dotted red line represents the connection between two conjugate EPs at a specific λ_R. The dotted blue square visually differentiates two alter topologies of Riemann surfaces around two conjugate EPs (for $\lambda_I > 0$ and $\lambda_I < 0$).

observed for different λ_I. Here, a coalescence between E_1 and E_2 occurs, when C vanishes, which refers to the appearance of a square-root branch point singularity that is associated with a complex conjugate pair of EPs in the complex λ plane given by

$$\lambda_{\text{EP}}^{+i} = -\frac{(\varepsilon_1 - \varepsilon_2)}{(\omega_1 - \omega_2) - 2i\sqrt{\kappa_1\kappa_2}}, \tag{3a}$$

$$\lambda_{\text{EP}}^{-i} = -\frac{(\varepsilon_1 - \varepsilon_2)}{(\omega_1 - \omega_2) + 2i\sqrt{\kappa_1\kappa_2}}. \tag{3b}$$

The formation of such a pair of conjugate EPs for specifically chosen parameters in $\mathcal{H}(\lambda)$, viz., $\varepsilon_1 = 1, \varepsilon_2 = 2, \omega_1 = 1, \omega_2 = -1, \kappa_1 = 0.5$, and $\kappa_2 = 0.1$, is shown in Fig. 1. Figures 1(a) and 1(b) show the Riemann surface distributions associated with Re(E) and Im(E) for the simultaneous variations of λ_R within [0.4, 0.56] and λ_I within [−0.17, 0.17], where two black crosses represent the pair of conjugate EPs appearing at $(0.4762 + i\,0.1063)$ and $(0.4762 - i\,0.1063)$ in the complex λ plane.

Now, if we want to implement optical systems with gain-loss based on the above Hamiltonian, then the situations $\lambda_I > 0$ and $\lambda_I < 0$ would essentially express two complementary optical systems concerning the gain-loss perturbation. Two associated coalescing levels are analytically connected via one of the two conjugate EPs in a particular system, whereas they are connected via the conjugate counterpart in the corresponding complementary system. In this context, the correlation between two complementary optical systems hosting such two conjugate EPs separately has the potential to explore an intriguing physical aspect associated with the chiral light dynamics, which has been investigated in this paper by exploiting the time-reversal ($\mathcal{T}$) symmetry, where $\mathcal{T} : \{x, t, i\} \rightarrow \{x, -t, -i\}$.

Based on the $\mathcal{T}$ symmetry, we explore the correlation between two complementary gain-loss assisted optical waveguides (WGs) to host two conjugate EPs. We design a framework of a planar dual-mode optical WG, where two complementary variants are realized based on two $\mathcal{T}$-symmetric complex potentials in the form of parameter-dependent unbalanced gain-loss profiles. We establish that the quasiguided modes of two complementary active WGs

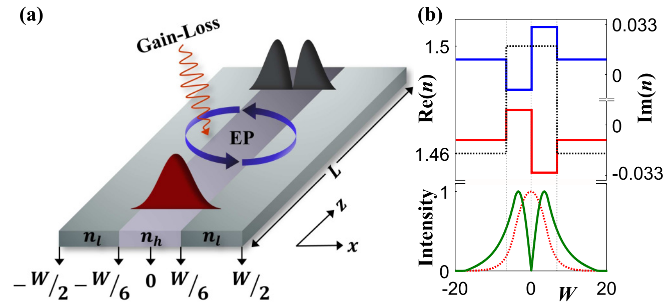

FIG. 2. (a) Schematic framework of the specialty gain-loss assisted WG system to realize two $\mathcal{T}$-symmetric complementary variants. (b) (Upper panel) Transverse profiles of $n_a(x)$ and $n_c(x)$; the dotted black line represents the variation of Re(n) associated with both, whereas the solid blue and red lines represent their respective Im(n) profiles for a specific cross section associated with $\gamma = 0.01$ and $\tau = 3.16$. (Lower panel) The normalized intensities of quasiguided ψ_F and ψ_H as shown by dotted red and solid green curves, respectively.

encounter two conjugate EPs in the respective parameter spaces associated with their $\mathcal{T}$-symmetric gain-loss profiles. Considering the dynamical parametric encirclement scheme of two conjugate EPs and implementing the constraints of $\mathcal{T}$ symmetry, we exclusively reveal the reverse-chiral response of two complementary variants of the designed WG. The proposed scheme has the potential to explore an unconventional platform for investigating the correlative response of two $\mathcal{T}$-symmetric optical systems around EP singularities.

II. RESULTS AND DISCUSSION

A. Design of two complementary waveguides to host parametrically encircled conjugate EPs

We configure a gain-loss assisted dual-mode planar step-index WG, occupying the regions $-W/2 \leqslant x \leqslant W/2$ and $0 \leqslant z \leqslant L$ along the transverse x and longitudinal z directions, respectively, as schematically shown in Fig. 2(a). The passive refractive indices of core and cladding are chosen as $n_h = 1.5$ and $n_l = 1.46$, respectively; whereas considering the normalized operating frequency $\omega = 1$, we set the effective width $W = 40$ (i.e., $20\lambda/\pi$; λ is the corresponding wavelength) and length $L = 18 \times 10^3$ in dimensionless units. The passive WG supports only two linearly polarized quasiguided scalar modes, i.e., the fundamental LP_{01} mode (say, ψ_F) and the first higher-order LP_{11} mode (say, ψ_H). Here, the modulation of gain-loss is controlled by a two-dimensional tunable parameter space based on a gain-loss coefficient γ with a ratio τ. Now, we consider two complimentary variants [say, $\text{WG}^{(a)}$ and $\text{WG}^{(c)}$ to represent the actual and complementary WG systems] concerning the $\mathcal{T}$-symmetric complex potentials in such a way that the transverse refractive index profiles of them [say, $n_a(x)$ and $n_c(x)$, respectively] can be written as

$$n_{a|c}(x) = \begin{cases} n_h - i\gamma \\ n_h + i\tau\gamma \\ n_l + i\gamma \end{cases} \left| \begin{array}{ll} n_h + i\gamma: & -W/6 \leqslant x \leqslant 0, \\ n_h - i\tau\gamma: & 0 \leqslant x \leqslant W/6, \\ n_l - i\gamma: & W/6 \leqslant |x| \leqslant W/2. \end{array} \right._{\mathcal{T}} \tag{4}$$

Figure 2(b) shows the transverse profiles of $n_a(x)$ and $n_c(x)$ along with normalized intensities of quasiguided ψ_F and ψ_H.

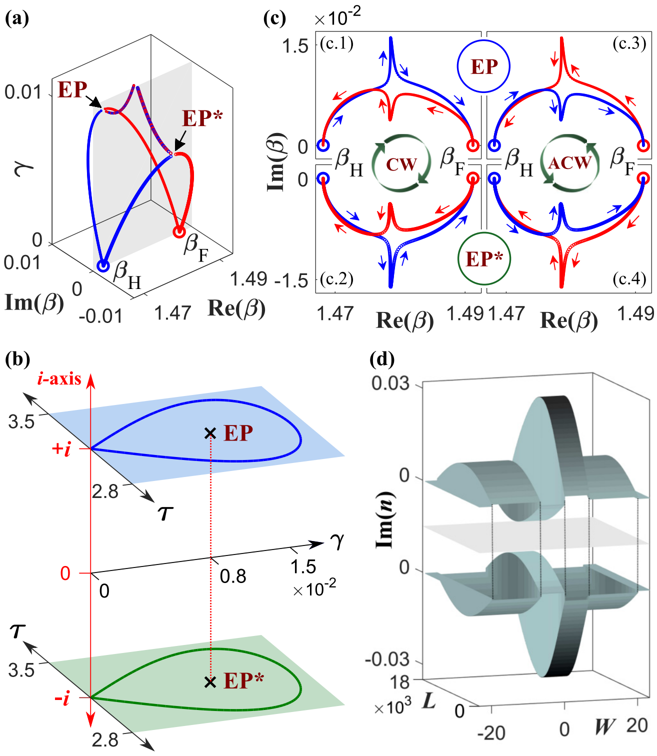

FIG. 3. (a) Coalescences of complex β_F (dotted red curve) and β_H (dotted blue curve) at $\gamma \approx 0.0082$ for a chosen $\tau = 3.16$, referring to the presence of conjugate EP and EP* in WG$^{(a)}$ and WG$^{(c)}$, respectively (as differentiated by the light-gray plane). The circular markers of respective colors represent the passive locations (when $\gamma = 0$) of β values (b) Encirclements of EP and EP* [following Eq. (5)] in their respective (γ, τ) planes associated with $\mathcal{T}$-symmetric complementary WG$^{(a)}$ and WG$^{(c)}$, respectively (as shown with respect to an additional i axis). (c) Adiabatic switching between β_F and β_H in the complex β plane, following the individual encirclements of EP and EP*, as shown in panel (b), in both CW [(c.1) and (c.2)] and ACW [(c.3) and (c.4)] directions. (d) The overall length-dependent variations of two complex conjugate Im(n) profiles associated with WG$^{(a)}$ and WG$^{(c)}$ after mapping the respective (γ, τ) parameter spaces [following Eq. (6)] to dynamically encircle EP and EP*, respectively.

Owing to $\mathcal{T}$ symmetry, two complementary WGs experience two exactly opposite gain-loss distribution concerning the transverse x direction.

Now, to encounter EPs in both the complementary WGs, we study the topological ARC-type interactions [3,11] between the propagation constants (β values) of coupled ψ_F and ψ_H [say, β_F and β_H, respectively; computed by solving the scalar modal equation $[\partial_x^2 + n^2(x)\omega^2 - \beta^2]\psi(x) = 0$ under approximation of small index difference] induced by the variation of gain-loss within a chosen range based on the control parameters γ and τ. For a specific $\tau = 3.16$, it is observed in Fig. 3(a) that β_F and β_H coalesce at $\gamma \approx 0.0082$, referring to the presence of second-order EPs at (0.0082, 3.16) in the (γ, τ) plane, for both the complementary variants. As can be seen here, the coalescence is observed along the positive Im(β) axis for WG$^{(a)}$ as it is loss dominated; however, in contrast, it is observed along the negative Im(β) axis for WG$^{(c)}$ as it is gain dominated. Thus, based on two $\mathcal{T}$-symmetric gain-loss profiles in the same passive WG, we encounter two EPs in the (γ, τ) plane. These two EPs can conveniently be defined as conjugate EPs, say EP and EP*, as their respective (γ, τ) parameter spaces are associated with two complex conjugates Im(n)-profiles corresponding to two complementary variants WG$^{(a)}$ and WG$^{(c)}$, respectively, of the designed passive WG.

To investigate the branch point behaviors of the pair of conjugate EPs toward their chiral features, we consider the stroboscopic encirclement processes of EP and EP* in their respective (γ, τ) planes associated with complementary WG$^{(a)}$ and WG$^{(c)}$. Accordingly, we implement the parametric equations

$$\gamma(\phi) = \gamma_0 \sin(\phi/2) \quad \text{and} \quad \tau(\phi) = \tau_{EP} + a \sin(\phi) \qquad (5)$$

to describe two closed loops, enclosing two conjugate EPs separately (with $\gamma_0 > \gamma_{EP}$), as shown in Fig. 3(b). Here, γ_{EP} $(= 0.0082)$ and τ_{EP} $(= 3.16)$ define the location of EP and EP* with respect to an additional i axis [$+i$ for WG$^{(a)}$, whereas $-i$ for WG$^{(c)}$]. $\gamma_0 = 0.015$ and $a = 0.3$, which are two characteristic parameters to control the closed variation of γ and τ over the angel $\phi \in [0, 2\pi]$; $\phi : 0 \to 2\pi$ enables the clockwise (CW) encirclement process, whereas $\phi : 2\pi \to 0$ enables the anticlockwise (ACW) encirclement process.

Now, we track the trajectories of complex β_F and β_H in Fig. 3(c) by following the stroboscopic variation of γ and τ along the chosen loops, where the left panel [3(c.1) and 3(c.2)] shows the trajectories for encirclements of EP and EP* in the CW direction and the right panel [3(c.3) and 3(c.4)] shows the same for the ACW encirclement processes. The hosting of such encirclement schemes in two $\mathcal{T}$-symmetric variants of the designed WG results in the adiabatic permutation between the initial positions of β_F and β_H in the complex β plane, as can be seen in Fig. 3(c), which reveals the second-order branch point behavior of the pair of conjugate EPs. Here, it is noticeable that the overall β trajectories due to encirclements of EP and EP* in any of the particular directions look like two mirror images with respect to the Im(β) axis. During the switching process, we can estimate the average loss encountered by any of the two particular modes as $\gamma^{av} = [\oint \text{Im}(\beta) d\phi]/2\pi$ with the corresponding adiabatic expectations of Im(β). Here, we observe that a specific mode, evolving with a lower γ_{av} due to encirclement of EP in a particular direction, experiences a higher γ_{av} due to encirclement of EP* in the same direction, and vice versa for the coupled counterpart mode; this fact is also evident from the trajectories shown in Fig. 3(c).

B. Dynamical encirclement of two conjugate EPs toward reverse-chiral response in asymmetric-mode-conversion process

To investigate the propagation of the quasiguided modes through the two $\mathcal{T}$-symmetric variants of the designed WG, we map the parameter spaces associated with EP and EP* throughout the length (z axis) of WG$^{(a)}$ and WG$^{(c)}$, respectively. Such a parameter space mapping, which allows a complete encirclement process ($\phi : 0 \to 2\pi$) to be equivalent to one complete pass of light through the waveguide ($z : 0 \to L$), enables the dynamical EP-encirclement process, where the control parameters vary with time or analogous length for

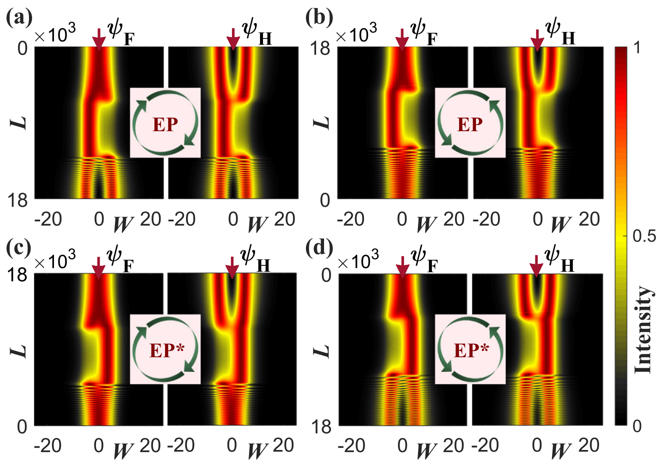

FIG. 4. (a), (b) Beam propagation simulation results through WG$^{(a)}$ for the dynamical encirclement of EP in (a) the CW direction, showing the conversions $\{\psi_F, \psi_H\} \to \psi_H$, and (b) the ACW direction, showing the conversions $\{\psi_F, \psi_H\} \to \psi_F$. (c), (d) Beam propagation simulation results through WG$^{(c)}$ for the dynamical encirclement of EP* in (c) the CW direction, showing the conversions $\{\psi_F, \psi_H\} \to \psi_F$, and (d) the ACW direction, showing the conversions $\{\psi_F, \psi_H\} \to \psi_H$.

optical systems (i.e., the t axis plays the role of the z axis; concerning the equivalence of the Helmholtz equation with the Schrödinger equation). Now, as the $\mathcal{T}$ symmetry enables the transformation $t \to -t$, we analogically consider the mapping of parameter spaces in two opposite directions along the z axis for two $\mathcal{T}$-symmetric variants of the designed WG. Accordingly, we implement the replacements

$$\phi = (2\pi z/L) \quad \text{and} \quad \phi = [2\pi(L - z)/L] \tag{6}$$

separately in Eq. (5) to realize the dynamical encirclements of EP and EP* with the simultaneous variations of $\{\gamma(z), \tau(z)\}$ in WG$^{(a)}$ and WG$^{(c)}$, respectively. The length dependence of associated complex conjugate Im(n) profiles are shown in the upper [for WG$^{(a)}$] and lower [for WG$^{(c)}$] panels of Fig. 3(d). Here, the CW dynamical encirclement process is equivalent to a complete propagation of light from $z = 0$ to $z = L$ (forward propagation along the $+z$ axis) for WG$^{(a)}$, whereas it is equivalent to a complete propagation of light from $z = L$ to $z = 0$ (backward propagation along the $-z$ axis) for WG$^{(c)}$. On the other hand the ACW dynamical encirclement process can be realized with a complete propagation from $z = L$ to $z = 0$ for WG$^{(a)}$ and from $z = 0$ to $z = L$ for WG$^{(c)}$. Here, CW and ACW variation of parameters for a specific encirclement process can be realized by changing the propagation directions of light through the respective variant.

In Fig. 4, we investigate the propagation of modes (along the z axis) in two $\mathcal{T}$-symmetric complementary variants of the designed WG due to dynamical encirclement processes of two respective conjugate EPs. To study the propagations of two quasiguided scalar modes ψ_F and ψ_H, we numerically solve the scalar beam propagation equation $[\partial_x^2 + \omega^2 \Delta n^2(x, z)]\psi(x, z) = -2i\omega\partial_z\psi(x, z)$ [with $\Delta n^2(x, z) \equiv n^2(x, z) - n_l^2$] by the split-step (Fourier) method under the paraxial approximation and the approximation of sufficiently slow (adiabatic) variation of Im(n) along the z axis. During the consideration of length dependence in the EP-encirclement process (dynamical), the induced relative gain-loss factors lead to the failure of the system's adiabaticity [despite the observed adiabatic switching process between the corresponding β values, as can be seen in Fig. 3(c)] with asymmetric population transfer among the corresponding coupled modes due to associated nonadiabatic corrections [24,25]. The associated light dynamics allows the adiabatic conversion of only one mode that evolves with a comparably lower γ_{av}, whereas its coupled counterpart evolves nonadiabatically and does not follow the adiabatic switching process.

In Fig. 4(a), we consider the CW dynamical encirclement of EP by launching light at $z = 0$ of WG$^{(a)}$ and observe that ψ_F is adiabatically converted to ψ_H, whereas ψ_H evolves nonadiabatically and remains in itself at $z = L$; i.e., only ψ_H dominates at the end of the encirclement process. However, while implementing the ACW dynamical encirclement of EP by considering the backward propagation of light ($z : L \to 0$) in WG$^{(a)}$, ψ_F dominates at the end of the encirclement process with a nonadiabatic transition of $\psi_F\,(\to \psi_F)$ and an adiabatic conversion of $\psi_H\,(\to \psi_F)$, as shown in Fig. 4(b). Thus, the dynamical encirclement of EP in WG$^{(a)}$ allows an asymmetric-mode-conversion process, where WG$^{(a)}$ exhibits the chiral response in the sense that it delivers two different dominating modes for encirclements in two different directions, irrespective of the inputs.

On the other hand, we observe an opposite chiral response in the associated-mode-conversion process upon considering the dynamical encirclement of EP* in WG$^{(c)}$. Here, the consideration of the encirclement in the CW direction with the excitation of modes from $z = L$ yields the dominating ψ_F at $z = 0$ with nonadiabatic and adiabatic conversions of $\psi_F\,(\to \psi_F)$ and $\psi_H\,(\to \psi_F)$, respectively, as shown in Fig. 4(c). However, the ACW dynamical encirclement of EP* results in adiabatic and nonadiabatic conversions of ψ_F and ψ_H excited from $z = 0$ to the dominating ψ_H at $z = L$, as can be seen in Fig. 4(d). Here, we also calculate the relative gain-loss factors to verify the beam propagation simulation results, where we observe that one of the modes that evolves with a lower γ_{av} transits adiabatically for all the cases.

Hence, based on the encirclement directions around two conjugate EPs, we establish the reverse-chiral response of two $\mathcal{T}$-symmetric variants of the designed WG. Interestingly, owing to constraints of $\mathcal{T}$ symmetry, two complementary variants deliver the same modes for the propagation of light in a particular direction through the designed WG. Here, the output intensities are indeed different for two variants, where the overall intensity decreases in loss-dominated WG$^{(a)}$, whereas it increases in gain-dominated WG$^{(c)}$. However, we renormalize the intensities at each step of propagation to show the beam propagations in Fig. 4 with proper visibility, and hence the variations of intensities are essentially scaled.

C. Validation of reverse-chiral response from the nonadiabatic correction terms

Here, a detail analytical treatment is presented to establish the reverse-chiral response of two complementary WGs by estimating the nonadiabatic correction factors associated with beam evolution processes. We assume that the 2×2 generic time-dependent Hamiltonian $\mathcal{H}(t)$, illustrating the proposed WG framework, depends on two time-dependent potential parameters $\mu_j(t)$ ($j = 1$ and 2) (analogically comparable to the parameters γ and τ), where two physical eigenvalues are assumed as $\beta_F^{ad}\{\mu_j(t)\}$ and $\beta_H^{ad}\{\mu_j(t)\}$ with two corresponding eigenvectors $\psi_F^{ad}\{\mu_j(t)\}$ and $\psi_H^{ad}\{\mu_j(t)\}$, respectively. Here, we can consider a similar parametric dependence for both WG$^{(a)}$ and WG$^{(c)}$ (however, exhibiting altered topologies), as they individually host EP and EP*, which are two conjugate singularities appearing from the eigenvalues of a generic Hamiltonian. The parameters $\mu_1(t)$ and $\mu_2(t)$ control the time-dependent nonadiabatic corrections in the solutions of time-dependent Schrödinger equation associated with $\mathcal{H}(t)$ [24]. Such nonadiabatic correction factors during the beam evolution processes led by the dynamical variation of parameters can be written as

$$\bigcap_{F/H\to H/F}^{NA} = \vartheta_{F/H\to H/F}^{NA} \exp\left\{(+/-)i\oint_0^T \Delta\beta_{F,H}^{ad}(\mu_j)dt\right\}, \quad (7)$$

with the pre-exponent term

$$\vartheta_{F/H\to H/F}^{NA} = \left\langle \psi_{F/H}^{ad}(\mu_j)\left|\sum_{j=1}^{2}\dot{\mu}_j\frac{\partial}{\partial\mu_j}\right|\psi_{H/F}^{ad}(\mu_j)\right\rangle. \quad (8)$$

Equation (7) represents the nonadiabatic correction factors for two transitions, simultaneously (via the associated suffix F/H $\to$ H/F), viz., $|\psi_F^{ad}\rangle \to |\psi_H^{ad}\rangle$ corresponding to the amplifying exponent term and $|\psi_H^{ad}\rangle \to |\psi_F^{ad}\rangle$ corresponding to the decaying exponent term. T represents the duration of the encirclement process. Now, the pre-exponent terms of $\bigcap_{F\to H}^{NA}$ and $\bigcap_{H\to F}^{NA}$ [i.e., $\vartheta_{F\to H}^{NA}$ and $\vartheta_{H\to F}^{NA}$, as given by Eq. 8] contain the time derivative of the two considered potential parameters, i.e., $\dot{\mu}_j$ ($j = 1$ and 2). Hence, the divergence in T associated with the exponential terms of $\bigcap_{F\to H}^{NA}$ and $\bigcap_{H\to F}^{NA}$ exceeds the decay of $1/T$ incorporated in the pre-exponents $\vartheta_{F\to H}^{NA}$ and $\vartheta_{H\to F}^{NA}$, respectively.

Here, the form of the factor $\Delta\beta_{F,H}^{ad} = (\beta_H^{ad} - \beta_F^{ad})$ [as appeared in the exponent of Eq. (7)] for two $\mathcal{T}$-symmetric WG variants can be written as

$$\Delta\beta_{F,H}^{ad}\{\mu_j(t)\} = \mathrm{Re}\big[\Delta\beta_{F,H}^{ad}(\mu_j)\big] \pm i\Delta\gamma_{F,H}^{ad}(\mu_j). \quad (9)$$

The plus and minus in Eq. (9) corresponds to the variants WG$^{(a)}$ and WG$^{(c)}$, respectively. The term $\Delta\gamma_{F,H}^{ad} = |\gamma_H^{av}| - |\gamma_F^{av}|$ represents the relative gain between the quasiguided modes, which would be alternatively positive and negative for two different encirclement directions [can be predicted from the associated adiabatic β trajectories shown in Fig. 3(c)]. The substitution of Eq. (9) in Eq. (7) gives a relative-gain-associated exponent part of $\bigcap_{F/H\to H/F}^{NA}$, i.e., $(-/+)\exp[\oint_0^T \Delta\gamma_{F,H}^{ad}(\mu_j)dt]$ for WG$^{(a)}$, and $(+/-)\exp[\oint_0^T \Delta\gamma_{F,H}^{ad}(\mu_j)dt]$ for WG$^{(c)}$, which is the key to detecting the final dominating output during the evolution of the beams.

Now, for the proposed variant WG$^{(a)}$, the dynamical encirclement of EP in the CW direction gives $\Delta\gamma_{F,H}^{ad} > 0$, which yields the nonadiabatic correction terms $\bigcap_{F\to H}^{NA} \to 0$ (converging) and $\bigcap_{H\to F}^{NA} \to \infty$ (diverging), while T $\to \infty$. On the other hand, the situation $\Delta\gamma_{F,H}^{ad} < 0$ during the dynamical EP encirclement in the ACW direction yields $\bigcap_{F\to H}^{NA} \to \infty$ and $\bigcap_{H\to F}^{NA} \to 0$. Here, the converging correction factors maintain the adiabaticity in the modal dynamics, whereas nonadiabaticity comes into the picture when the correction factors diverge. Thus, during the dynamical encirclement of EP in the CW direction, $\bigcap_{F\to H}^{NA} \to 0$ allows the adiabatic conversion of $|\psi_F^{ad}\rangle$ into $|\psi_H^{ad}\rangle$ and $\bigcap_{H\to F}^{NA} \to \infty$ forces $|\psi_H^{ad}\rangle$ to remain as $|\psi_H^{ad}\rangle$ beyond the adiabatic expectations. On the other hand, the vice-versa conditions during the dynamical EP encirclement in the ACW direction allows the nonadiabatic evolution of $|\psi_F^{ad}\rangle$ ($\to |\psi_F^{ad}\rangle$) and the adiabatic conversion of $|\psi_H^{ad}\rangle$ ($\to |\psi_F^{ad}\rangle$).

In contrast, while we consider the variant WG$^{(c)}$, the condition $\Delta\gamma_{F,H}^{ad} > 0$ during the dynamical encirclement of EP* in the CW direction gives $\bigcap_{F\to H}^{NA} \to \infty$ and $\bigcap_{H\to F}^{NA} \to 0$, whereas the condition $\Delta\gamma_{F,H}^{ad} < 0$ during the dynamical encirclement of EP* in the ACW direction gives $\bigcap_{F\to H}^{NA} \to 0$ and $\bigcap_{H\to F}^{NA} \to \infty$. Hence, WG$^{(c)}$ allows the nonadiabatic evolution of $|\psi_F^{ad}\rangle$ ($\to |\psi_F^{ad}\rangle$) and the adiabatic conversion of $|\psi_H^{ad}\rangle$ ($\to |\psi_F^{ad}\rangle$) during the CW EP*-encirclement scheme, whereas it allows the adiabatic conversion of $|\psi_F^{ad}\rangle$ ($\to |\psi_H^{ad}\rangle$) and the nonadiabatic evolution of $|\psi_H^{ad}\rangle$ ($\to |\psi_H^{ad}\rangle$) during the ACW EP*-encirclement scheme.

Hence, the above analytical treatment establishes the reverse-chiral response of two conjugate EPs in two $\mathcal{T}$-symmetric complementary WG variants. Here, one can predict the dominating output based on the relative gain factor in the nonadiabatic corrections associated with beam dynamics, where the relative gain dependence re-establishes the fact that only the least-decaying mode obeys the adiabatic expectation. The analytically predicted adiabatic and nonadiabatic transitions for different encirclement schemes can be verified by observing the beam propagation results shown in Fig. 4.

III. CONCLUSION

In summary, we exclusively propose the concept of conjugate EPs and report the hosting of such a pair of conjugate EPs in two complementary variants of a dual-mode planar waveguide based on two $\mathcal{T}$-symmetric optical potentials in terms of complex refractive index profiles. Here, two waveguide variants experience unbalanced gain-loss profiles in such a way that their refractive index profiles are complex conjugate and correlated by $\mathcal{T}$ symmetry. We implement the dynamical encirclements of two conjugate EPs in their respective parameter spaces and reveal an asymmetric-mode-conversion scheme for both variants, where light is converted into different particular dominating modes for two different encirclement directions in terms of the direction of light propagation. Based on the constraints of $\mathcal{T}$ symmetry, we establish the reverse-chiral response of two complementary variants of the designed waveguide, concerning the direction of the encirclement process, where the individual dynamical encirclements of two conjugate EPs in two opposite encirclement directions result in the delivery of the same dominating modes by the respective waveguide variants. The findings enriched with the physics of conjugate EPs will certainly open up a potential platform to investigate the inherent correlations of optical responses of two $\mathcal{T}$-symmetric systems toward unconventional light manipulation mechanisms for a wide range of integrated (or on-chip) device applications. Furthermore, in the context of nonreciprocal transmission through such complementary optical systems in the presence of local nonlinearity, the basis of $\mathcal{T}$ symmetry would certainly be of interest and also open to explore in exploiting the functionalities of conjugate EPs.

ACKNOWLEDGMENTS

A.L. and S.G. acknowledge the financial support from the Science and Engineering Research Board (SERB), Ministry of Science and Technology, under the Early Career Research Scheme [Grant No. ECR/2017/000491], Government of India. S.D. acknowledges the financial support from the Ministry of Education, Government of India.

[1] B. Midya, H. Zhao, and L. Feng, Nat. Commun. **9**, 2674 (2018).
[2] T. Kato, *Perturbation Theory for Linear Operators* (Springer, Berlin, 1966).
[3] W. D. Heiss, Phys. Rev. E **61**, 929 (2000).
[4] M.-A. Miri and A. Alù, Science **363**, eaar7709 (2019).
[5] Ş. K. Özdemir, S. Rotter, F. Nori, and L. Yang, Nat. Mater. **18**, 783 (2019).
[6] J. Wiersig, Phys. Rev. A **93**, 033809 (2016).
[7] W. Chen, Ş. Kaya Özdemir, G. Zhao, J. Wiersig, and L. Yang, Nature (London) **548**, 192 (2017).
[8] H. Xu, D. Mason, L. Jiang, and J. G. E. Harris, Nature (London) **537**, 80 (2016).
[9] C. Dembowski, B. Dietz, H.-D. Gräf, H. L. Harney, A. Heine, W. D. Heiss, and A. Richter, Phys. Rev. E **69**, 056216 (2004).
[10] A. Laha, D. Beniwal, S. Dey, A. Biswas, and S. Ghosh, Phys. Rev. A **101**, 063829 (2020).
[11] A. Laha, D. Beniwal, and S. Ghosh, Phys. Rev. A **103**, 023526 (2021).
[12] H. Hodaei, A. U. Hassan, W. E. Hayenga, M. A. Miri, D. N. Christodoulides, and M. Khajavikhan, Opt. Lett. **41**, 3049 (2016).
[13] C. Wang, W. R. Sweeney, A. D. Stone, and L. Yang, Science **373**, 1261 (2021).
[14] A. A. Zyablovsky, E. S. Andrianov, and A. A. Pukhov, Sci. Rep. **6**, 29709 (2016).
[15] J. Doppler, A. A. Mailybaev, J. Böhm, U. Kuhl, A. Girschik, F. Libisch, T. J. Milburn, P. Rabl, N. Moiseyev, and S. Rotter, Nature (London) **537**, 76 (2016).
[16] A. Laha, A. Biswas, and S. Ghosh, Phys. Rev. Appl. **10**, 054008 (2018).
[17] X.-L. Zhang, S. Wang, B. Hou, and C. T. Chan, Phys. Rev. X **8**, 021066 (2018).
[18] A. Laha, S. Dey, H. K. Gandhi, A. Biswas, and S. Ghosh, ACS Photonics **7**, 967 (2020).
[19] R. Thomas, H. Li, F. M. Ellis, and T. Kottos, Phys. Rev. A **94**, 043829 (2016).
[20] W. D. Heiss, J. Phys. A: Math. Theor. **45**, 444016 (2012).
[21] W. D. Heiss and H. L. Harney, Eur. Phys. J. D **17**, 149 (2001).
[22] A. Hashemi, S. M. Rezaei, S. K. Özdemir, and R. El-Ganainy, APL Photonics **6**, 040803 (2021).
[23] H. L. Harney and W. D. Heiss, Eur. Phys. J. D **29**, 429 (2004).
[24] I. Gilary, A. A. Mailybaev, and N. Moiseyev, Phys. Rev. A **88**, 010102(R) (2013).
[25] T. J. Milburn, J. Doppler, C. A. Holmes, S. Portolan, S. Rotter, and P. Rabl, Phys. Rev. A **92**, 052124 (2015).